

Chad M. Michener¹, Chris Kirkup², Bahar Rahsepar², Janani S. Iyer², John Abel², Ken Leidal², Archit Khosla², Ben Trotter², Mary Lin², Murray Resnick², Ben Glass², Ilan Wapinski² & Fedaa Najdawi²

¹Cleveland Clinic, Cleveland, Ohio ²PathAI, Boston, Massachusetts

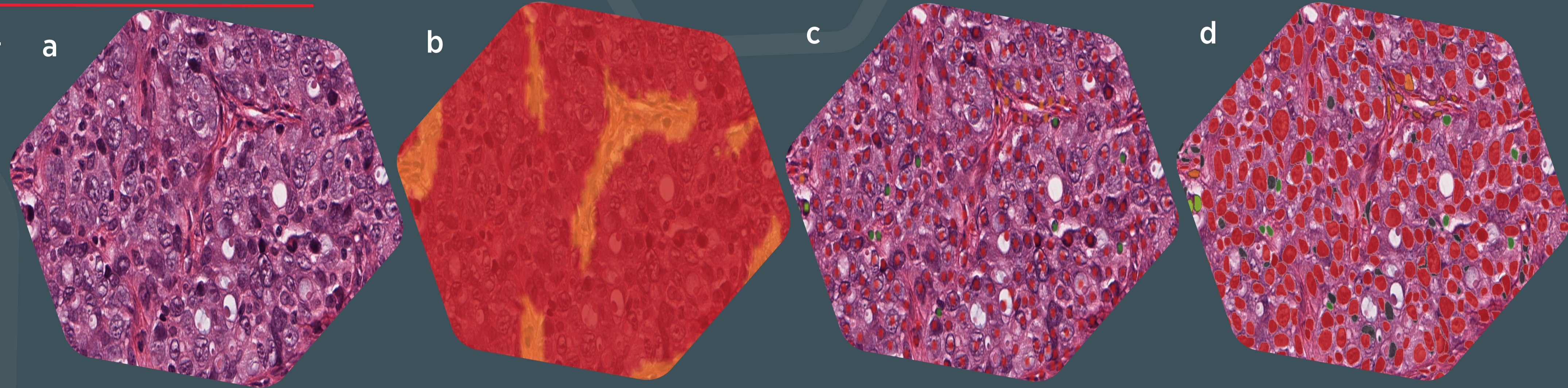
STUDY BACKGROUND

Ovarian carcinoma is a leading driver of cancer-related mortality in women, but predicting long-term survival at diagnosis remains a challenge¹. The majority of advanced stage cases are of the aggressive high-grade serous carcinoma (HGSC) subtype².

Features of both the tumor microenvironment as well as cancer cell nuclei have both been shown to affect clinical outcome in several cancer types, including ovarian cancer³⁻⁶. Here we demonstrate that AI-powered pathology can classify cells and tissue regions in the high-grade serous carcinoma (HGSC) tumor microenvironment, and reveal nuclear morphology associated with patient outcomes, directly from digitized hematoxylin and eosin (H&E)-stained whole slide images (WSI).

MODEL-GENERATED OVERLAYS

Figure 3. PathAI model-generated overlays. a) H&E-stained HGSC WSI. b) Tissue-level overlay showing model predictions for cancer stroma (orange), and cancer epithelium (red). c) Cell-level overlay showing model predictions for cancer epithelial cells (red), lymphocytes (green), fibroblasts (orange), and plasma cells (light green). d) Nuclear segmentation overlay showing heterogeneity in nuclear size and shape.



METHODS

- Machine learning (ML) models were trained using H&E WSI of ovarian carcinoma samples from both publicly available (e.g. TCGA) and proprietary sources (Total N=352 slides from 257 subjects). ML models were trained to label tissue regions (cancer epithelium, stroma, necrosis) and cell types (cancer epithelial cells, fibroblasts, and inflammatory cells) using 138,632 pathologist-provided annotations (Fig. 1).

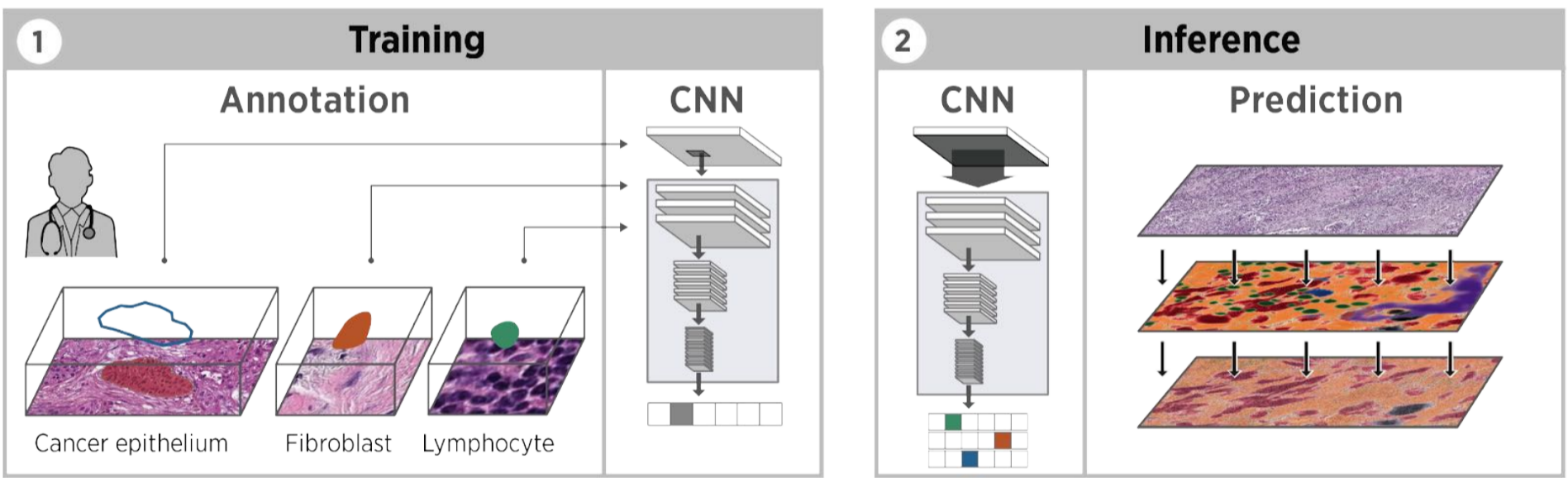


Figure 1. Schematic illustrating convolutional neural network (CNN) model development approach for pixel-level feature predictions.

- A separate nuclear segmentation was deployed on H&E WSI from 93 subjects to characterize nuclear morphology at single-pixel resolution (Fig. 2).

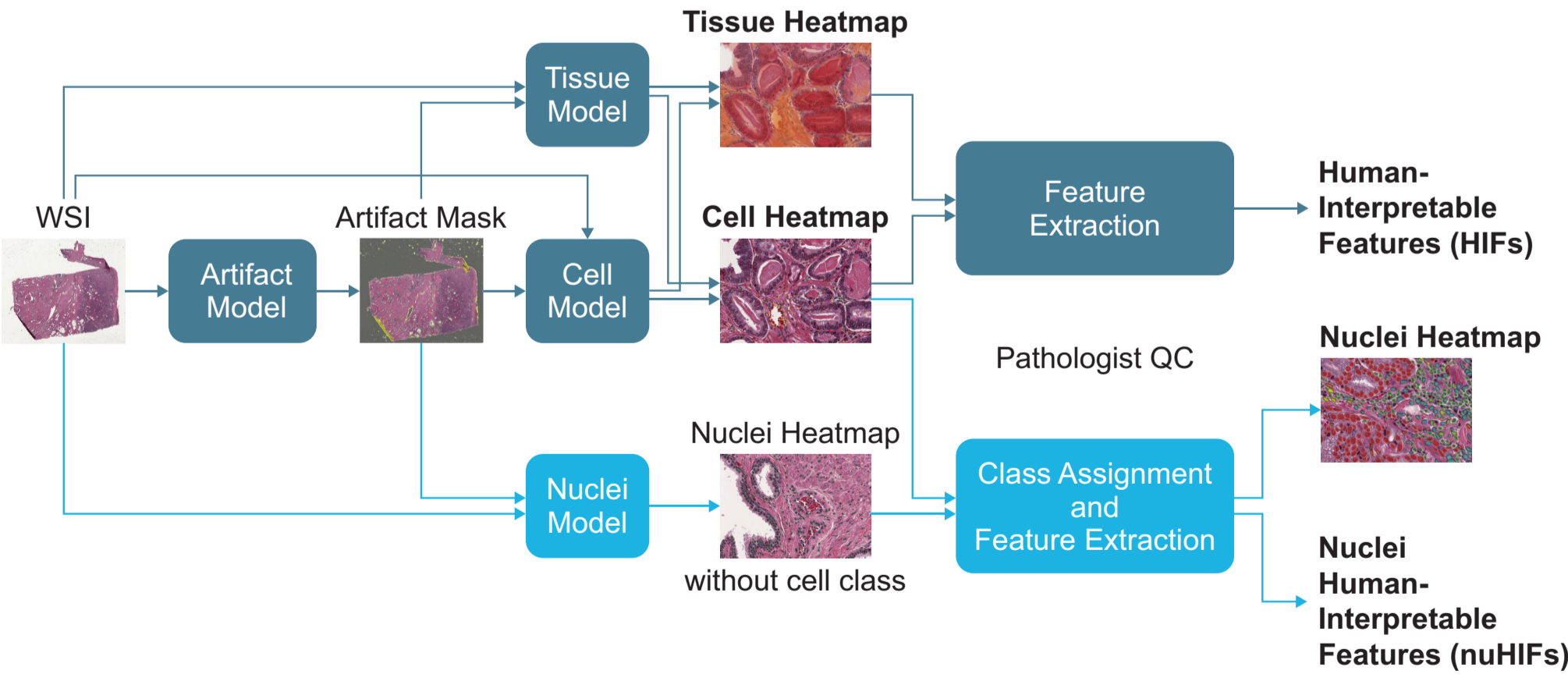


Figure 2. Integration of cell, tissue, and nuclear model workflows. The nuclear segmentation model segments all nuclei in H&E WSI; the cell model is then used to assign cell class to each identified nucleus. Human-interpretable features (HIFs) extracted from cell and tissue heatmaps include cell counts and area proportions; nuclei HIFs include nuclear size, shape, and staining intensity.

- Survival and clinically relevant statuses were regressed vs. nuclear features using univariate Cox or logistic regressions. False discovery rate correction was applied using the Benjamini-Hochberg procedure.

RESULTS

MODEL PERFORMANCE EVALUATION

- Five pathologists exhaustively annotated 240 frames of smaller tissue regions (300 x 300 pixels) to produce consensus ground truth cell labels. Model predictions (Fig. 3a-c) were compared with pathologist consensus in these frames using Pearson correlation. Individual pathologist predictions were also compared with pathologist consensus.
- Model performance is particularly strong in quantification of cancer epithelial cells and lymphocytes; weaker performance in fibroblasts and macrophages reflects greater inter-pathologist variability in these cell class predictions (Fig. 4).

Cell Class	Pearson (95% CI)	
	Model vs Consensus n=240	Annotator vs Consensus n=240
Cancer epithelial cell	0.85 (0.82, 0.87)	0.92 (0.89, 0.95)
Lymphocyte	0.75 (0.70, 0.78)	0.78 (0.70, 0.85)
Fibroblast	0.54 (0.47, 0.60)	0.66 (0.61, 0.70)
Macrophage	0.36 (0.28, 0.44)	0.50 (0.49, 0.52)
Plasma cell	0.67 (0.62, 0.72)	0.82 (0.75, 0.88)

Figure 4. Cell model performance evaluation. Model performance was assessed in a held-out test set (not used in model training) comprising 49 WSIs.

ML-QUANTIFIED NUCLEAR FEATURES ASSOCIATED WITH ANEUPLOIDY AND OVERALL SURVIVAL

- Analysis of nuclear morphology revealed that greater inter-nuclear variation in staining intensity and minor axis length (Fig. 3d) were associated with reduced overall survival, reflecting the effect of variability in chromatin characteristics (corrected p=0.023, Hazard Ratio (HR) = 2.51) and inter-nuclear heterogeneity in shape and size across a slide (corrected p=0.035, HR=2.11), respectively (Fig. 5).

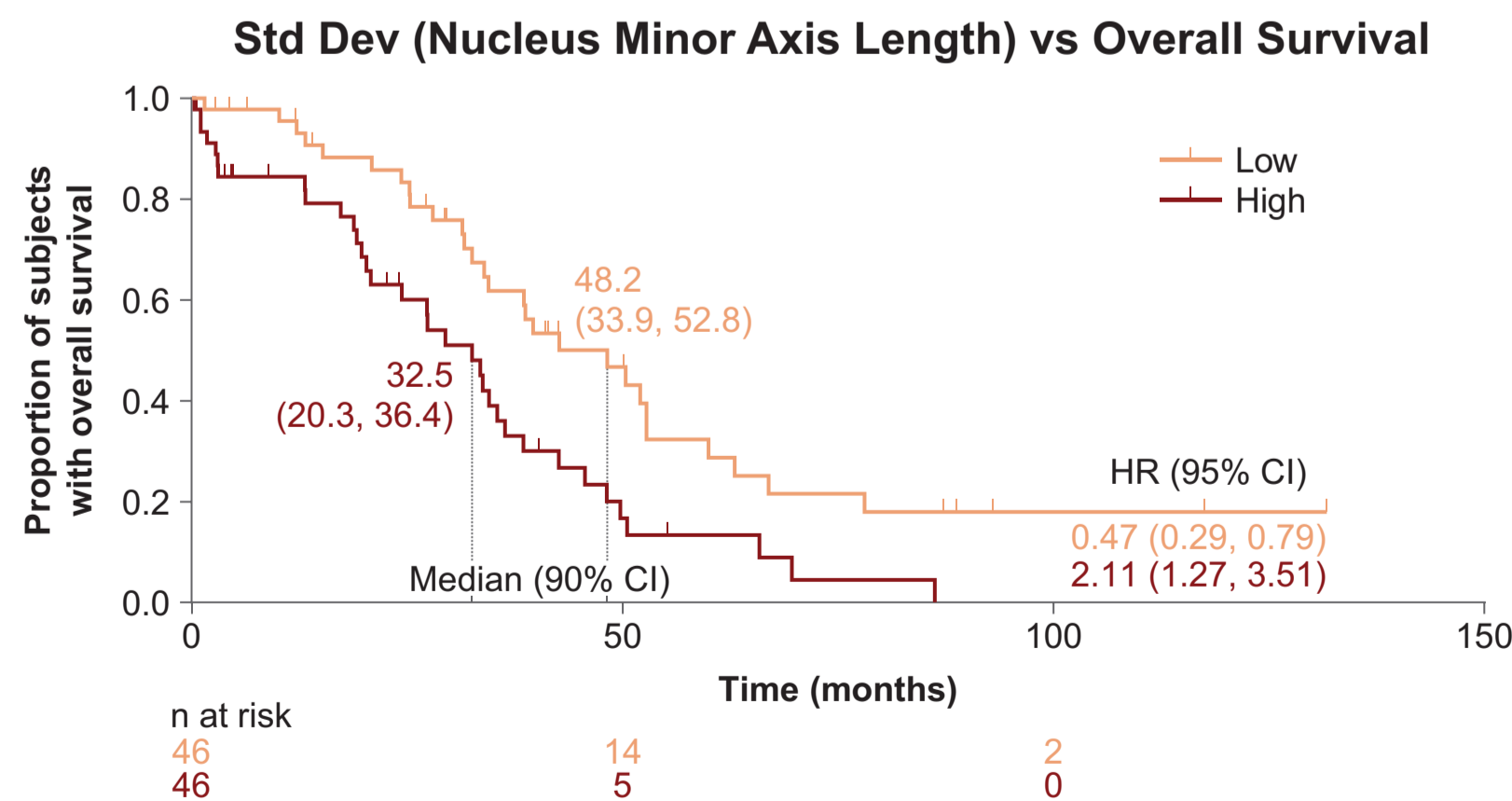


Figure 5. Greater variability in nuclear minor axis length associated with reduced overall survival. Kaplan-Meier analysis.

- Greater variation in nucleus minor axis length was also correlated with increased number of aneuploidy events involving gains in chromosome arms (Spearman correlation r=0.41, p<0.001) (Fig. 6).

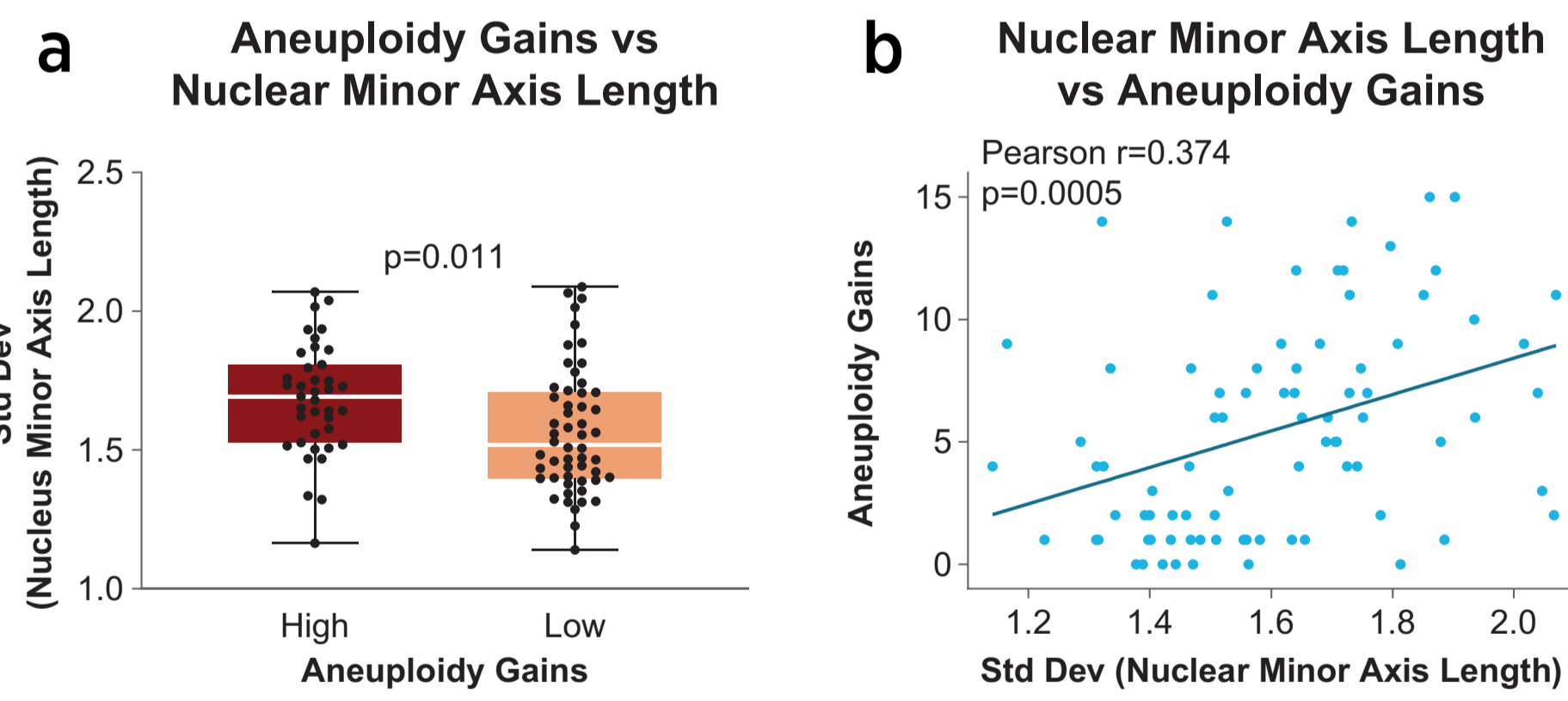
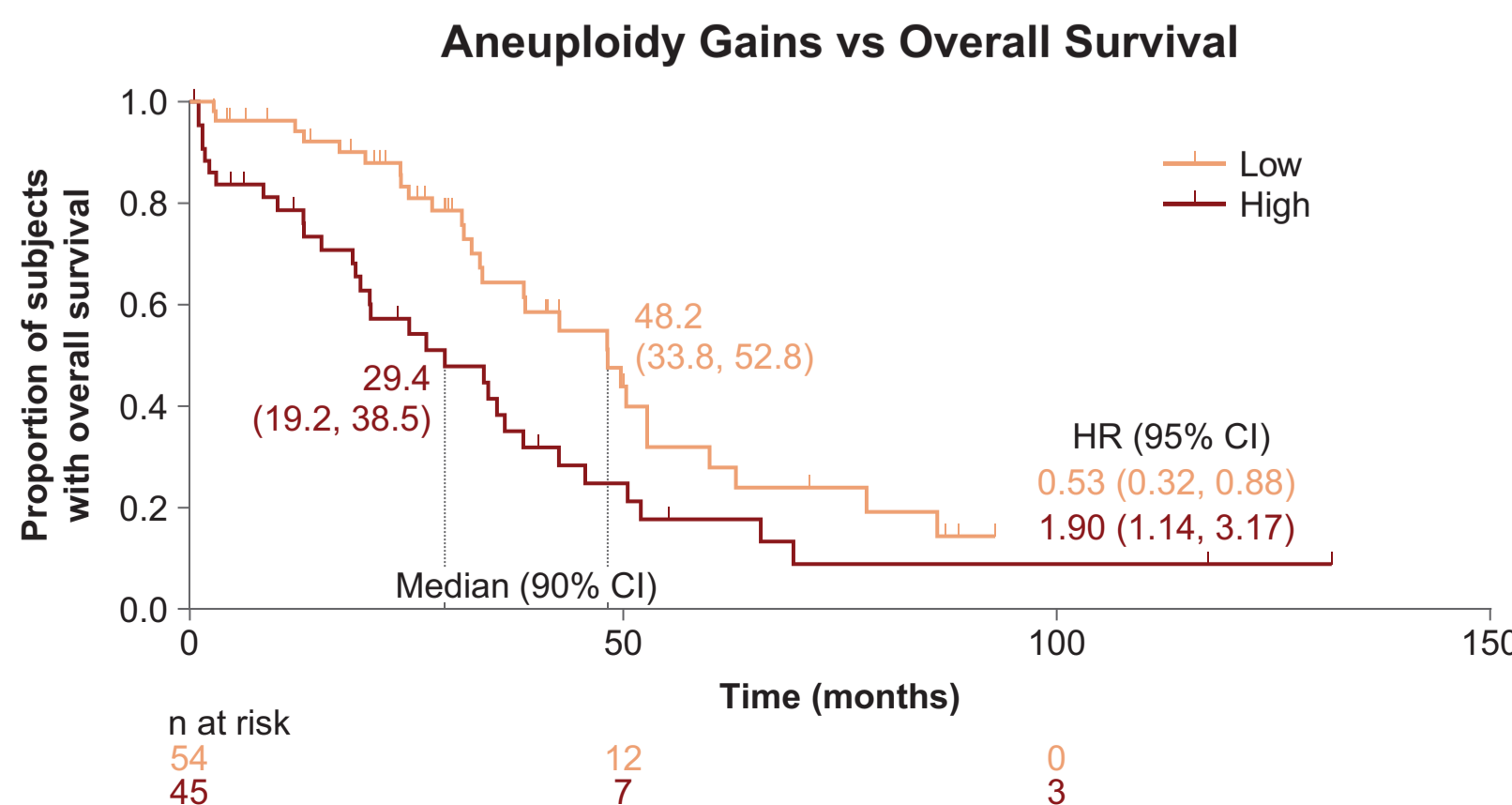


Figure 6. Correlation of greater variability in nuclear minor axis length with increased aneuploidy events involving gains in chromosome arms. a) Stratified boxplot; b) continuous correlation.

- Aneuploidy events involving gains in chromosome arms were in turn predictive of reduced overall survival (corrected p=0.042, HR=1.90) (Fig. 7).

Figure 7. Aneuploidy events were predictive of reduced overall survival. Kaplan-Meier analysis.



CONCLUSIONS

- ML model classification of ovarian cancer cell types and tissue regions is concordant with manual pathologist consensus.
- ML-based analysis further reveals a relationship between cancer cell nuclear morphological diversity (pleomorphism and chromatin variability), aneuploidy, and patient prognosis.
- The ovarian carcinoma model developed in this study could be applied in future studies to classify various molecular subtypes of HGSC.
- Moreover, follow up studies could also leverage digital pathology to investigate response to various targeted therapies such as immunotherapy and PARP inhibitors based on ML-quantified features of the tumor microenvironment and nuclear morphology, potentially enabling strategies for matching of patients with appropriate targeted therapies and clinical trials.

CONTACT

Chad M. Michener: michenc@ccf.org
Fedaa Najdawi: fedaa.najdawi@pathai.com

REFERENCES

1. Momenimovahed, Z, et al. Int J Womens Health. 2019; 11:287-299.
2. Bowtell, DD, et al. Nat Rev Cancer. 2015; 15:668-679.
3. Diao, JA, et al. Nat Comms. 2021; 12:1613.
4. Mahmood, T, et al. J. Pers. Med. 2021; 11:515.
5. Launonen, IM, et al. Nat Comms. 2022; 13, 835.
6. Sengupta, D, et al. PLoS One 2022; 17: e0261181.

ACKNOWLEDGMENTS

We thank Bioscience Communications for assistance with figure design. This poster template was developed by SciStories LLC. <https://scistories.com/>

